A two-directional approach for grating based differential phase contrast imaging using hard x-rays

C. Kottler and C. David
Laboratory for Micro- and Nanotechnology, Paul Scherrer Institut, 5232 Villigen PSI Switzerland
christian.kottler@psi.ch

F. Pfeiffer and O. Bunk
Swiss Light Source, Paul Scherrer Institut, 5232 Villigen PSI, Switzerland

Abstract: We report on a two-directional approach for grating based x-ray differential phase contrast imaging. In order to retrieve good quality and artifact-free phase images for quantitative analysis and image processing, particular emphasis is put on the algorithm for proper phase retrieval. Examples of application are discussed that demonstrate the functionality of the method even in cases where the one-dimensional phase integration fails completely.

© 2007 Optical Society of America

OCIS codes: (050.1950) Diffraction gratings; (100.5070) Phase retrieval; (340.7450) X-ray interferometry; (340.7440) X-ray imaging

References and links

1. R. Fitzgerald, "Phase-Sensitive X-Ray Imaging," Phys. Today **53**, 23–27 (2000).
2. A. Momose, "Phase-sensitive imaging and phase tomography using X-ray interferometers," Opt. Express **11**, 2303–2314 (2003).
3. A. Momose, "Demonstration of X-Ray Talbot Interferometry," Jpn. J. Appl. Phys. **42**, L866–L868 (2003).
4. V.A. Somenkov, A.K. Tkalich, and S.S. Shilstein, "Refraction contrast in x-ray introscopy" Sov. J. Tech. Phys. **61**, 197–201 (1991).
5. V.V. Protopopov, and J. Sobota, "X-ray dark-field refraction-contrast imaging of micro-objects," Opt. Commun. **213**, 267–279 (2002).
6. U. Bonse and M. Hart, "An X-ray interferometer," Appl. Phys. Lett. **6**, 155–156 (1965).
7. A. Momose, T. Takeda, Y. Itai, and K. Hirano, "Phase-contrast X-ray computed tomography for observing biological soft tissues," Nature Med. **2**, 473–475 (1996).
8. V. N. Ingal and E. A. Beliaevskaya, "X-ray plane-wave topography observation of the phase contrast from a non-crystalline object," J. Phys. D **28**, 2314–2317 (1995).
9. T. J. Davis, D. Gao, T. E. Gureyev, A. W. Stevenson, and S. W. Wilkins, "Phase-contrast imaging of weakly absorbing materials using hard X-rays," Nature (London) **373**, 595–598 (1995).
10. D. Chapman, W. Thomlinson, R. E. Johnston, D. Washburn, E. Pisano, N. Gmür, Z. Zhong, R. Menk, F. Arfelli, and D. Sayers, "Diffraction enhanced x-ray imaging," Phys. Med. Biol. **42**, 2015–2025 (1997).
11. S. W. Wilkins, T. E. Gureyev, D. Gao, A. Pogany, and A. W. Stevenson, "Phase-contrast imaging using polychromatic hard X-rays," Nature (London) **384**, 335–337 (1996).
12. F. Pfeiffer, T. Weitkamp, O. Bunk, and C. David, "Phase retrieval and differential phase-contrast imaging with low brilliance X-ray sources," Nature Physics **2**, 258 (2006).
13. T. Weitkamp, A. Diaz, C. David, F. Pfeiffer, M. Stampanoni, P. Cloetens, and E. Ziegler "X-ray phase imaging with grating interferometer," Opt. Express **13**, 6296–6304 (2005).
14. K. Creath, "Phase-measurement Interferometry Techniques," in *Progress In Optics XXVI*, E. Wolf, ed., pp. 349–393 (Elsevier Science, 1988).
15. C. David, B. Nöhammer, H. H. Solak, and E. Ziegler, "Differential x-ray phase contrast imaging using a shearing interferometer," Appl. Phys. Lett. **81**, 3287–3289 (2002).

#76936 - $15.00 USD Received 14 November 2006; revised 21 December 2006; accepted 19 January 2007

16. T. Weitkamp, B. Nöhammer, A. Diaz, C. David, and E. Ziegler, "X-ray wavefront analysis and optics characterization with a grating interferometer," Appl. Phys. Lett. **86**, 054,101 (2005).
17. Huber goniometer head type #1003, HUBER Diffraktionstechnik GmbH & Co. KG, Germany.
18. M. Born and E. Wolf, *Principles of Optics*, sixth ed. (Pergamon Press, Oxford, England, 1993).
19. In fact, the quantity measured is not the absolute displacement $\langle \Delta x \rangle_{real} \propto \frac{\partial \Phi}{\partial x}$ but $\langle \Delta x \rangle = (\langle \Delta x \rangle_{real} \mod p_2)$ because a steep phase gradient can shift the fringes more than one period p_2. This phenomenon is known as phase-wrapping.
20. M.R. Arnison, K.G. Larkin, C.J.R. Sheppard, N.I. Smith, and C.J. Cogswell, "Linear phase imaging using differential interference contrast microscopy," J. Microsc. **214**, 7–12 (2004).

1. Introduction

In the past years the interest has grown for x-ray imaging of samples for a variety of applications such as medicine, industrial/food quality inspection of products and non-destructive testing. In particular, phase imaging has become the method of choice for radiography of weakly absorbing materials, such as soft tissue samples because of its higher contrast when compared to conventional absorption radiography [1–3]. These phase-sensitive techniques require x-rays of high spatial and/or temporal coherence. Therefore, they are either implemented in combination with crystal or multilayer optics, at synchrotron facilities or they use low-power micro-focus x-ray tubes [4–11]. Some techniques also require in vacuum samples or have a limited field of view. These constraints lead to either a high cost or insignificant flux, hindering the breakthrough of the method as a standard and complementary x-ray imaging scheme for a wide variety of applications.

As recently demonstrated in [12, 13], a new technique that uses transmission gratings can overcome the obstacle of spatial and temporal incoherent x-ray tube radiation. Thus, quantitative phase-contrast images can be retrieved of centimeter sized samples. Taking advantage of the so called phase-stepping data acquisition mode [14–16], this technique provides not only the advantage of phase sensitive imaging but also complementary conventional absorption radiography. This method has the potential to provide phase-sensitive imaging for routine operation for any application even at existing x-ray tube based systems.

The quantity that serves as imaging information is not the wave-front phase profile $\Phi(x,y)$, but its first derivative along the axis perpendicular to the grating lines $\Phi_x \equiv \frac{\partial \Phi(x,y)}{\partial x}$. Thus this technique is called differential phase-contrast (DPC) imaging. When it comes to applications such as in biology or medicine the quality of images becomes an important issue because it decides whether the relevant details can be interpreted properly. Quantitative analysis and signal processing require retrieval of the wave front profile $\Phi(x,y)$. In principle, this can be done by a trivial one-dimensional integration. Nevertheless, in practice this integration very often results in phase images that suffer from unfavorable artifacts. In this work a two dimensional method for phase retrieval that takes advantage of combining images of local phase gradients along two orthogonal directions is described. We demonstrate that this approach improves the quality of images even in cases where the simple integration approach is not applicable. Especially when the boundary conditions are not completely known as is the case for samples that are larger than the field of view.

2. Grating interferometer set-up and differential phase images

As displayed in Fig. 1 our set-up consists of a laboratory x-ray tube and three gratings: a source grating G_0, a phase grating G_1 and an analyzer absorption grating G_2. The periods are $p_0 = 73\ \mu$m, $p_1 = 3.89\ \mu$m and $p_2 = 2.0\ \mu$m, respectively. The whole set-up was mounted on adjustable rails on an optical bench which was installed inside a radiation shielding box. The x-ray generator used for the experiments was a Seifert ID 3000 with a Tungsten (W) line focus tube (DX-W8x0.4-L) operated at 35 kV and 30 mA. The source grating G_0 was mounted close

#76936 - $15.00 USD Received 14 November 2006; revised 21 December 2006; accepted 19 January 2007
(C) 2007 OSA

to the x-ray source spot and directly onto the x-ray tube exit window. The distance between G_0 and G_1 was l =1.6 m, the distance between G_1 and G_2 was d =4.5 cm. The gratings were made from Si wafers using standard photolithography techniques and subsequent electroplating to fill the grooves with gold (G_0 and G_2). The gratings size (G_1 and G_2) and thus the achievable field of view of 64 x 64 mm^2 is determined by the maximum size on native 100 mm Si wafers. The x-ray detector consisted of a CsI-scintillator screen (thickness: 150 μm), demagnifying optics and a cooled charge coupled device (CCD) detector. The spatial resolution was $\approx$0.1 mm. The scintillator screen extended the field of view determined by the grating size.

The source grating G_0, an absorbing mask of gold with transmission slits of 23 μm width and p_0 =73 μm pitch creates an array of individually coherent, but mutually incoherent sources and is essential for the successfulness of the grating interferometer with polychromatic high-power x-ray tubes. With the appropriate combination of the grating periodicity and alignment substantial spatial coherence is achieved and thus the total source size only affects the spatial resolution but not phase sensitivity. In our set-up the effective width of the x-ray tube source spot of 0.8 mm$\times$0.4 mm (horizontal $\times$ vertical), and the distance between the source spot, sample and detector l and d (Fig. 1) resulted in a smearing on the order of a few microns, and therefore is negligible when compared to the spatial resolution ($\approx$0.1 mm).

The gratings were mounted on brackets and were installed on small motorized goniometer heads [17]. They could be aligned both with respect to their rotation around the beam axis and their translation along the beam axis. The sample was mounted on a motorized *xy*-translation stage and an additional rotation stage around the beam axis (*z*-axis).

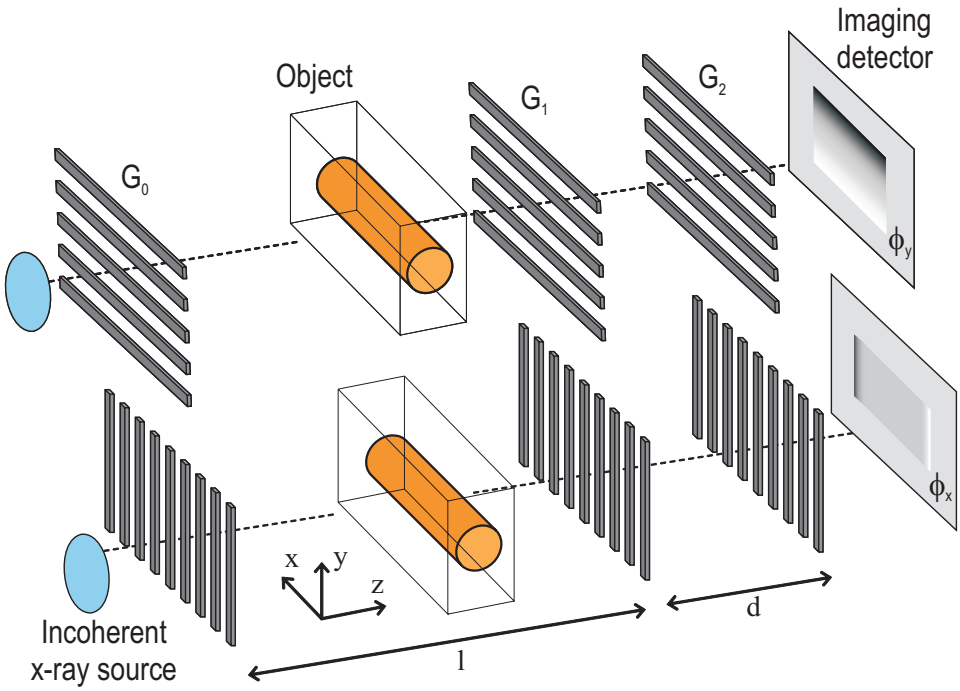

Fig. 1. Schematic overview of the interferometer set-up consisting of an x-ray tube, a source grating G_0, a phase grating G_1, an analyzer grating G_2 and an imaging detector. DPC images along the *x*- and *y*-axis can be measured by alignment of the gratings in vertical (bottom) and horizontal (top) direction, respectively. In order to measure DPC images for both directions *x* and *y*, in our experiments the sample was turned by 90° instead of the gratings.

#76936 - $15.00 USD Received 14 November 2006; revised 21 December 2006; accepted 19 January 2007
(C) 2007 OSA

The gratings G_1 and G_2 form the phase sensitive interferometer. G_1 is a grating made of Si with equal line widths and spaces between. The transmissive lines have a phase shift on the order of $\Delta\phi \approx \pi$. The amount of phase shift $\Delta\phi$ through the grating lines depends on their thickness (in our experiment: 35 μm) and on the x-ray wavelength λ. If G_1 is illuminated by a plane wave, a periodic interference pattern of intensity is formed downstream that changes as a function of the distance from G_1. For $\Delta\phi(\lambda \equiv \lambda_0) = \pi$ a periodic pattern of linear fringes parallel to the grating lines is observed at the Talbot distance ($d = p_1^2/8\lambda_0$). The pitch of these fringes equals half of the periodicity of the beam splitter grating (p_1).

If an object is placed in front of the interferometer on the one hand the intensity of the incident plane wave is reduced according to the absorption of the object. On the other hand the refractivity of the object causes local distortions of the wave front profile and thus a slight deflection of the beam. This angle of local deflection α is given by [18]

$$\alpha(x) = \frac{\lambda}{2\pi}\frac{\partial\Phi(x)}{\partial x} \quad , \tag{1}$$

where $\Phi(x)$ is the phase profile as a function of the transverse direction x. This slight angle of incidence α on G_1 results in a local displacement of the interference fringes $\Delta x = \alpha \cdot d$ at the distance d downstream from G_1. Therefore, the local phase-shift $\Phi(x)$ given by the index of refraction of the object can be translated into a local displacement Δx of the interference fringes. Since the direct determination of the exact position of these fringes requires detectors with spatial resolution in the sub-micron range a second grating G_2 is introduced to determine the average displacement Δx of the fringes within a detector pixel. G_2 is a mask of equidistant bars of gold and transmitting slits. The periodicity p_2 equals the periodicity of the undistorted interference pattern. If G_2 is stepped perpendicularly to the grating bars (x-direction, see Fig. 1, bottom) and individual pictures are taken in each position the intensity of each pixel becomes an oscillating function of G_2 position. The position of the maximum in this periodic signal is proportional to the average displacement Δx, and thus to the local phase gradient $\frac{\partial\Phi}{\partial x}$ (Eq. 1, [19]). Therefore, determining the average displacement shift $\langle\Delta x\rangle$ for each pixel yields an image of the phase gradient. Furthermore, the average over one period of this intensity oscillation is proportional to the transmitted intensity through the object and thus provides the absorption radiograph. Taking advantage of this phase-stepping acquisition mode both, the absorption image and the local phase gradient image can be measured at the same time.

3. Phase integration algorithm

Phase retrieval by simple one dimensional integration along the x-axis may fail to give phase images of satisfactory quality. There are three main reasons that cause artifacts thereby. First, if the object to be investigated is bigger than the field of view, the boundary conditions and thus the starting wave front profile $\Phi(x = 0, y)$ for the integration are unknown. This can be seen in Fig. 2(d) and 2(e) where broad shadows are caused by parts of the object (the flower's petal) extending past the boarder of the image. The second cause for artifacts is noise in the phase gradient images. Statistical errors in the determination of $\langle\Delta x\rangle$ of course depend on counting statistics and the number of G_2 phase-steps performed. Statistical uncertainties propagate throughout the integration and thus cause stripes parallel to the direction of integration (see Fig 3(d) and 3(e)). Third, phase-wrapping causes similar artifacts as image noise. The conch in Fig. 4(d) and 4(e) gives an example of a case where the object fits into the field of view and the phase image is acquired with high statistics, however the integration is not without artifacts.

To overcome these problems we developed an approach that combines information from two independent directions of integration. The algorithm is similar to the one presented by Arnison et. al. [20] for visible light. The idea is to measure the phase gradient image for both directions x

#76936 - $15.00 USD Received 14 November 2006; revised 21 December 2006; accepted 19 January 2007
(C) 2007 OSA

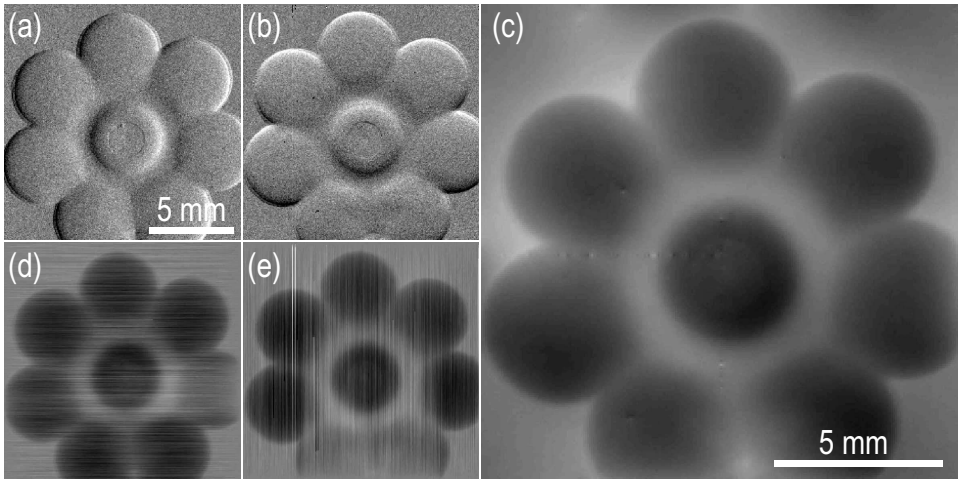

Fig. 2. DPC image of a flower-like shape made of plastic for *x*- (a) and *y*-direction (b) of the gradient. (d) and (e) show the corresponding integrated phase images, respectively. Since some of the petals do not completely fit into the field of view shadow-like artifacts arise therein upon integration . (c) shows the image obtained with the 2D algorithm.

and y, thus $\Phi_x(x,y)$ and $\Phi_y(x,y)$. The latter was acquired by rotating the sample by 90° around the beam axis (see Fig. 1).

We define the complex field $g(x,y)$ as

$$g(x,y) = \Phi_x(x,y) + i\Phi_y(x,y) \equiv \frac{\partial \Phi}{\partial x}(x,y) + i\frac{\partial \Phi}{\partial y}(x,y). \tag{2}$$

Then, its two-dimensional Fourier transform can be written as

$$\mathscr{F}\left[g(x,y)\right](k,l) \equiv \iint_{-\infty}^{+\infty} g(x,y)\cdot e^{-2\pi i(kx+ly)}dxdy = 2\pi i(k+il)\cdot \mathscr{F}\left[\Phi(x,y)\right](k,l), \tag{3}$$

using the Fourier derivative theorem and where (k,l) represent the reciprocal space coordinates corresponding to (x,y). Therefore, the wave front profile $\Phi(x,y)$ can be obtained by inverse Fourier transform Eq. (3), yielding:

$$\Phi(x,y) = \mathscr{F}^{-1}\left[\frac{\mathscr{F}\left[\Phi_x + i\Phi_y\right](k,l)}{2\pi i(k+il)}\right](x,y). \tag{4}$$

4. Examples

Successful applications of this integration algorithm are shown in Fig. 2, 3 and 4. When the sample is bigger than the field of view the integration fails. The particular problem in images 2(d) and 2(e) is the broad shadow that occurs from the petal overlapping the boundary of the integration. Our method overcomes this problem and yields the appropriate phase image 2(c). The algorithm can deal with the problem from the unknown boundary conditions because it takes the two-dimensional phase gradient into account and thus reconstructs the phase profile in a self-consistent way.

#76936 - $15.00 USD Received 14 November 2006; revised 21 December 2006; accepted 19 January 2007
(C) 2007 OSA

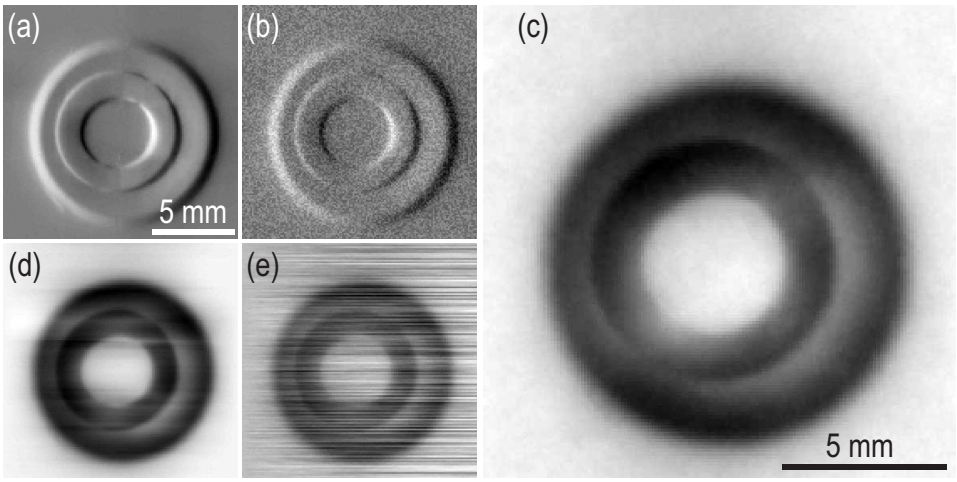

Fig. 3. DPC images of two concentrically arranged plastic rings acquired with high (a) and reduced (b) counting statistics, both of them for *x*-direction of the gradient. The corresponding integrated phase images are shown in (d) and (e), respectively. (c) shows the image obtained with the 2D algorithm applied on the lower statistics data.

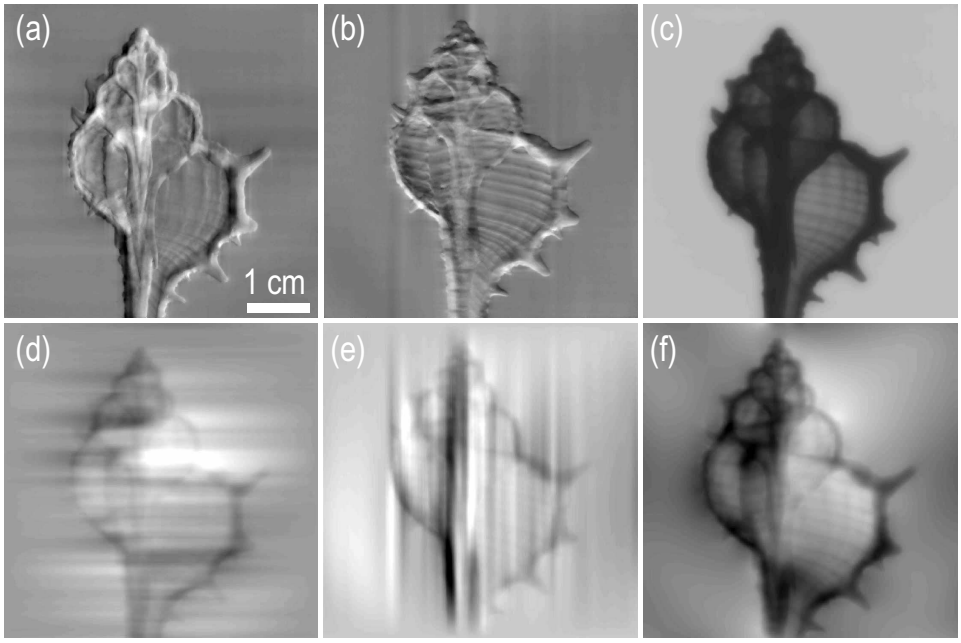

Fig. 4. DPC image of a conch for *x*- (a) and *y*-direction (b) of the gradient. (d) and (e) show their integrated phase images, respectively. (f) shows the image from the 2D algorithm and in comparison (c) shows the absorption image.

#76936 - $15.00 USD Received 14 November 2006; revised 21 December 2006; accepted 19 January 2007
(C) 2007 OSA

Examples for acquisition of DPC images with different statistics are shown in Fig. 3(a) and Fig. 3(b), 64 phase-steps and 8 phase-steps, respectively. In both cases the exposure time was 5s per step. In the lower statistics case the integrated image Fig. 3(e) suffers from horizontal stripes. Indeed, the phase image obtained likewise but with higher statistics is of much better quality. However, with the lower statistics data and the new method a much clearer image is obtained, Fig. 3(c). In the example presented here, the problem of image noise could be solved by acquiring better statistics. Nevertheless, for samples where the signal-to-noise ratio is inherently small (samples with weak phase contrast) this new method prevails.

Finally, in Fig. 4 an example is given that suffers from phase-wrapping. For both *x*- and *y*-direction in the integrated images (Fig. 4(d) and 4(e)) not only do stripes appear but also spots of very low or very high intensity. Indeed, using our algorithm these artifacts are eliminated (Fig. 4(f)) and thus the detailed structure of the conch is revealed.

5. Conclusion

The two-directional approach for grating interferometry and the according algorithm improves phase retrieval from DPC images. The method can deal with the problem of noise in DPC images that generally causes stripes upon integration. Furthermore, it was shown that our method also yields appropriate phase images in cases where linear integration is not possible, such as for phase-wrapping and large objects.

Acknowledgments

This work was supported by the Swiss Commission for Technology and Innovation KTI/CTI under contract 7796.2 DCPP-NM.

#76936 - $15.00 USD Received 14 November 2006; revised 21 December 2006; accepted 19 January 2007
(C) 2007 OSA